Journal of the Serbian Society for Computational Mechanics / Vol. 17 / No. 1, 2023 / pp 56-70
(10.24874/jsscm.2023.17.01.04)

NUMERICAL SIMULATIONS OF THE INFLUENCE OF VARIOUS PARAMETERS ON HEAT TRANSFER AND FLOW SEPARATION IN SUPERSONIC COOLED NOZZLES

Bensayah Khaled[1, 2, *] and Kamri Khadidja[2]

[1] Interprofessional Complex Research in Aerothermochemistry CORIA UMR 6614 CNRS, INSA of Rouen, France
e-mail: k.bensayah@lagh-univ.dz
[2] Laboratory of Mechanics, Department of Mechanical Engineering, University of Laghouat, Algeria
e-mail: Kha.kamri@yahoo.com
**corresponding author*

Abstract

In rocket engine nozzle design, flow separation is essential and, given the high temperatures and pressures in the thrust chamber, regenerative cooling is critical for maintaining the nozzle wall's integrity. This passage provides a summary of an in-depth numerical analysis of boundary layer separation and heat transfer within a 30°-15° cooled nozzle. The performance of the SST-V turbulence model under these conditions is assessed numerically. A variety of factors are investigated, including wall temperature, turbulent Prandtl number, and constant specific heat ratios (spanning 1.31 to 1.4 for constant fluid properties of N2O, CH4, Cl2, and air). Furthermore, variable specific heat ratios (from 1.39 to 1.66 for variable fluid properties of air, CH4, O2, and Helium) are examined, along with other parameters that affect the location of separated flow and the local wall heat transfer.

Keywords: Regenerative cooling nozzle, separation position, SST-V turbulence model, supersonic flow.

1. Introduction

Accelerating turbulent flows exhibit unique fluid mechanics and heat transfer characteristics compared to non-accelerating cases. Supersonic nozzle flows are of particular interest for both design and fundamental research purposes, prompting numerous global studies to investigate and enhance the understanding of heat transfer phenomena in rocket nozzles. This process is highly sensitive to various factors, including combustion, injection schemes, turbulence, and others. Heat transfer in nozzles takes place under substantial pressure gradients and extremely high stagnation temperatures, resulting in a combination of two components: a convective element and an additional radiative component.

At first, the focus of research and analysis was primarily directed towards examining convective occurrences in pipes and conical nozzles featuring a low angle of divergence, as well

as low pressure and stagnation temperature. This area has been studied by Saunders and Calder (1953), Ragsdale and Smith (1959), Baron and Durgin (1954), and Kolozsi (1958).

Back et al. (1963) conducted an important parametric study, in which they experimentally examined the impact of various parameters - including stagnation pressure and temperature, as well as boundary layer thickness - on convective heat transfer. Their findings showed that the coefficient of heat transfer increases with increasing stagnation pressure in cases involving turbulent boundary layers. However, the effects of stagnation temperature remain unclear. The researchers also observed that a thinner boundary layer at the inlet results in a higher heat transfer coefficient.

Leccese et al. (2018) made similar observations in their study, which aimed to compare convective and radiative heat transfer in a thrust chamber. The authors discovered that the heat flux decreases along the chamber due to thickening of the boundary layer, which hinders convective contribution while radiative contribution remains constant. In addition, they also examined how combustion mixture affects these processes using two mixtures - (O/CH4) and (O/H).

Leccese et al. (2018) found that the chemical elements only affect radiation, whereas convection depends solely on the thermal conductivity of the mixture. As a result, heat transfer was greater in the case of (O/H). The researchers also made similar observations to Back et al. (1963) regarding increased chamber pressure having an effect on convective heat transfer. With regard to wall temperature, Leccese et al. reported that increasing wall temperature leads to a decrease in convective flow due to small differences between flow and wall temperatures.

Arnold et al. (2009) performed an experimental study to investigate parameters affecting cooling film efficiency in a model high-pressure combustion chamber. The authors specifically examined the impact of film blowing and the ratio between injection speed and gas speed. They found that increasing film blowing was responsible for improved cooling film efficiency, while both an increased ratio of injection speed to gas speed and Reynolds number of the slot contributed to enhancing cooling film efficiency as well.

Miranda et al. (2011) analyzed the impact of flow film on heat transfer in a thrust chamber, considering factors such as the composition and flow characteristics of the cooling liquid. The study's results revealed that hydrogen is better at reducing heat transferred to walls than an (O/f) mixture for fixed wall temperatures. However, sometimes it may be necessary to use the cooler mixture (O/f) due to over-cooling generated by hydrogen.

Other factors have also been investigated, such as injection angle and slot height (Kurtbas (2008)), as well as chemical reactions (Betti et al. (2014)). Kim et al. (2012) examined the effects of altitude on heat transfer and discovered that the transfer decreases with increasing altitude due to a decrease in air density. Daimon et al. (2012) stressed the importance of considering combustion byproducts and flame-wall interactions when modeling heat transfer in a thrust chamber, an observation later confirmed by Frank and Pfitzner (2017).

Despite numerous studies on this subject, there has not yet been a comprehensive analysis of the phenomenon or development of appropriate methodologies. To fill some gaps, we conducted numerical simulations to explore heat transfer characteristics associated with turbulent flow through converging-diverging nozzles and investigate how various parameters affect fluid flow distribution under adiabatic and isothermal wall conditions. Our study focused particularly on understanding how parameters such as turbulent Prandtl number, wall temperature, specific heat ratio γ), impact both wall heat transfer distribution and static pressure at separation position.

2. Modeling turbulence and numerical techniques

2.1 Modeling of turbulence

In order to avoid computational issues associated with using the precise source term for turbulent kinetic energy k, a modified version of the Shear Stress Transport (SST) model known as SST-V is employed. This approach combines the strengths of both k − ϵ and k − ω models. In SST-V, the local measurement of vorticity, as described by Vieser et al. (2002) and Tong and Luke (2004), is responsible for generating k. By utilizing this formulation, a dependable estimate of the source term's production can be obtained in the boundary layer, as shown in equation 2 by Leccese et al. (2018).

$$\tau_{ij} = \mu_t \left(\frac{\partial U_i}{\partial x_j} + \frac{\partial U_j}{\partial x_i} - \frac{2}{3} \frac{\partial U_k}{\partial x_k} \delta_{ij} \right) - \frac{2}{3} \rho k \delta_{ij} \tag{1}$$

$$\tau_{ij} \frac{\partial U_i}{\partial x_j} = \mu_t \Omega^2 - \frac{2}{3} \rho k \delta_{ij} \frac{\partial U_i}{\partial x_j} \tag{2}$$

The model uses two additional transport equations to describe the turbulence:

$$\frac{D}{Dt}(\rho k) = \tau_{ij} \frac{\partial U_i}{\partial x_j} - \beta^* \rho \omega k + \frac{\partial}{\partial x_j} \left((\mu + \sigma_k \mu_t) \frac{\partial k}{\partial x_j} \right) \tag{3}$$

$$\frac{D}{Dt}(\rho \omega) = \frac{\gamma \rho}{\mu_t} \tau_{ij} \frac{\partial U_i}{\partial x_j} - \beta \rho \omega^2 + \frac{\partial}{\partial x_j} \left[\left(\mu + \sigma_{\omega_1} \mu_t \right) \frac{\partial \omega}{\partial x_j} \right] + 2\rho (1 - F_1) \sigma_{\omega 2} \frac{1}{\omega} \frac{\partial k}{\partial x_j} \frac{\partial \omega}{\partial x_j} \tag{4}$$

The Lagrangian derivative is defined as $D/Dt = \partial/\partial t + u_j \partial/\partial x_j$. The blending function F_1 can be expressed using the following equation:

$$F_1 = \tanh \left\{ \left(min \left(max \left(\frac{\sqrt{k}}{0.09 \omega y}, \frac{500 \mu}{\rho \omega y^2} \right), \frac{4 \rho \sigma_{\omega 2} k}{C D_{k\omega} y^2} \right) \right)^4 \right\} \tag{5}$$

In this case, the term $CD_{k\omega}$ refers to cross-diffusion included in equation (4). The eddy viscosity is calculated using the following formula: $\mu t = \rho a_1 k / \max(a_1 \omega, \Omega F_2)$, where F_2 is a function that is only applied to the boundary layer.

$$F_2 = \tanh \left(\left(max \left(\frac{2\sqrt{k}}{0.09 \omega y}, \frac{500 \nu}{y^2 \omega} \right) \right)^2 \right)$$

2.2 Realizability condition

Reynolds stress and mean strain tensor are connected through the Boussinesq assumption, which can be expressed as:

$$-\rho \widetilde{u_i} \widetilde{u}_j = 2 C_\mu \rho \frac{k^2}{\varepsilon} \left(S_{ij} - \frac{1}{3} S_{ll} \right) - \frac{2}{3} \rho k \delta_{ij} \tag{6}$$

With $C\mu = 0.09$, the shear stress is proportional to turbulent kinetic energy in the presence of a strong pressure gradient as per Bradshaw's findings, where $-\widetilde{uv} \approx \sqrt{C_\mu k}$. Taking both observations into account, Cμ can be expressed as:

$$C_\mu = min\left(0.09, \frac{1}{A_0 + A_s(S^2 + A_\Omega\Omega^2)^{1/2}}\right) \tag{7}$$

with

$$\begin{cases} S = \frac{1}{\omega\beta^*}\sqrt{2S_{ij}S_{ij} - \frac{2}{3}S_{kk}^2}, S_{ij} = \frac{1}{2}\left(\frac{\partial u_i}{\partial x_j} + \frac{\partial u_j}{\partial x_i}\right) \\ \Omega = \frac{1}{\omega\beta^*}\sqrt{2\Omega_{ij}\Omega_{ij}}, \Omega_{ij} = \frac{1}{2}\left(\frac{\partial u_i}{\partial x_j} - \frac{\partial u_j}{\partial x_i}\right) \end{cases} \tag{8}$$

When $A_0 = 0, A_s = 2\sqrt{3}$, and $A_\Omega = 0$, the Bradshaw coefficient (0.31) is substituted with $\sqrt{C_\mu}$ in equation (7), which formulates the eddy viscosity.

2.3 Numerical method

The equations are presented in a conservative form that separates contributions from both viscous and non-viscous sources. The S_0 terms are treated separately.

$$\frac{\partial U}{\partial t} + \frac{\partial F(U)}{\partial x} + \frac{\partial G(U)}{\partial y} = \frac{\partial F_v(U)}{\partial x} + \frac{\partial G_v(U)}{\partial y} + S_0(U) \tag{9}$$

The vector U denotes the conservative variables,

$$U = \begin{pmatrix} \bar{\rho} \\ \bar{\rho}\tilde{u} \\ \bar{\rho}\tilde{v} \\ \bar{\rho}\tilde{E} \\ \bar{\rho}k \\ \bar{\rho}\omega \end{pmatrix}, \quad S_0 = \begin{pmatrix} 0 \\ 0 \\ 0 \\ 0 \\ H_k \\ H_\omega \end{pmatrix} \tag{10}$$

Here, the terms F and G represent the inviscid flux, whereas Fv and Gv refer to the viscous vectors,

$$F = \begin{pmatrix} \bar{\rho}\tilde{u} \\ \bar{\rho}\tilde{u}\tilde{u} + p^* \\ \bar{\rho}\tilde{u}\tilde{u} \\ \left(\bar{\rho}\tilde{E} + p^*\right)\tilde{\rho} \\ \bar{\rho}\tilde{u}k \\ \bar{\rho}\tilde{u}\omega \end{pmatrix}, \qquad G = \begin{pmatrix} \bar{\rho}\tilde{v} \\ \bar{\rho}\tilde{v}\tilde{u} \\ \bar{\rho}\tilde{v}\tilde{v} + p^* \\ \left(\bar{\rho}\tilde{E} + p^*\right)\tilde{v} \\ \bar{\rho}\tilde{v}k \\ \bar{\rho}\tilde{v}\omega \end{pmatrix} \tag{11}$$

In this context, $\bar{\rho}$ represents the density of the fluid, while $\tilde{u}$ and $\tilde{v}$ denote its x- and y-components of velocity. The total energy is represented by $\tilde{E}$, while p denotes static pressure derived from perfect gas equation of state.

$$p = (\gamma - 1)\bar{\rho}\left(\tilde{E} - \frac{(\tilde{u}^2 + \tilde{v}^2)}{2} - k\right) \tag{12}$$

The expressions for the viscous fluxes, F_v and G_v are:

$$F_v = \begin{pmatrix} 0 \\ \tilde{\sigma}_{xx} \\ \tilde{\sigma}_{xy} \\ \tilde{\sigma}_{xx}\tilde{u} + \tilde{\sigma}_{xy}\tilde{v} - \bar{q}_x \\ \tilde{\sigma}_{kx} \\ \tilde{\sigma}_{\omega x} \end{pmatrix}, \qquad G_v = \begin{pmatrix} 0 \\ \tilde{\sigma}_{xx} \\ \tilde{\sigma}_{yy} \\ \tilde{\sigma}_{xy}\tilde{u} + \tilde{\sigma}_{yy}\tilde{v} - \bar{q}_y \\ \tilde{\sigma}_{ky} \\ \tilde{\sigma}_{\omega y} \end{pmatrix} \tag{13}$$

$\tilde{\sigma}$ represents the stress-tensor and $\bar{q}$ denotes the vector of heat flux. To solve the equations of Navier-Stokes numerically, a finite volume predictor-corrector method is employed on a computational domain defined by variables ζ and η, which correspond to transformed coordinates of physical domain.

MacCormack's (2012) combined explicit-implicit technique is employed to address the novel equation system. This approach exhibits second-order accuracy in both spatial and temporal dimensions. Steger and Warming (1979) adapted the basic discretization process for convective fluxes to account for the physical properties of information propagation. In regions with shock waves, flux splitting is diminished to first order. The integration of axisymmetric source terms occurs at the center of each control volume for both ζ and η directional sweeps, while the viscous terms are also centered.

An explicit discretization is combined with a numerical implicit approximation, which has no stability constraints, to achieve a steady-state solution with minimal iterations. To solve the block pentadiagonal system in the η direction, a generalized Thomas method with LU decomposition is utilized, followed by a line Gauss-Seidel relaxation technique in the ζ direction. The method is iterative, and due to the diagonally dominant system, a convergent steady solution can be obtained in a relatively small number of time steps, each involving a double backward-forward sweep in the flow direction. This approach allows for the use of unrestricted time step values. C.F.L values greater than 15 (Campbell and Farley, 1960) have been employed in numerical computations. This paper primarily presents the results of the current study, while a comprehensive explanation of the numerical method and associated equations can be found in the reference (Bensayah and Kamri, 2022).

3. Results and analysis

3.1 Validation and boundary conditions

The research employed a conical nozzle contour presented in Fig. 1.b, which was identical to previous studies conducted by Bensayah et al. (2014) and Cuffel et al. (1968). The study applied prescribed total pressure and temperature at the inlet while maintaining axisymmetric conditions along the nozzle symmetry line. Initially, adiabatic wall conditions were considered for model validation purposes, followed by specific modifications based on each case being studied.

Figure 1.a displays various radial locations of computed and measured static pressure from Cuffel et al. (1968), demonstrating significant radial variation with a gradient that closely mirrors axial static-pressure gradient. Figure 1.b shows that gas expands faster along the wall than centerline due to compressive turning of flow associated with static-pressure increase behind tangent between throat circular arc and conical diverging portion in Fig. 1.a.

Flow overturning near the wall is observed because of high angular motion maintained by flow near small curvature radius region close to throat; thus, flow lines slope towards downstream conical walls. Mach number contours depict shock production commencement related to

compressive twisting of flow where weak oblique shock wave originates, propagating downstream intersecting centerline at x = 8 cm.

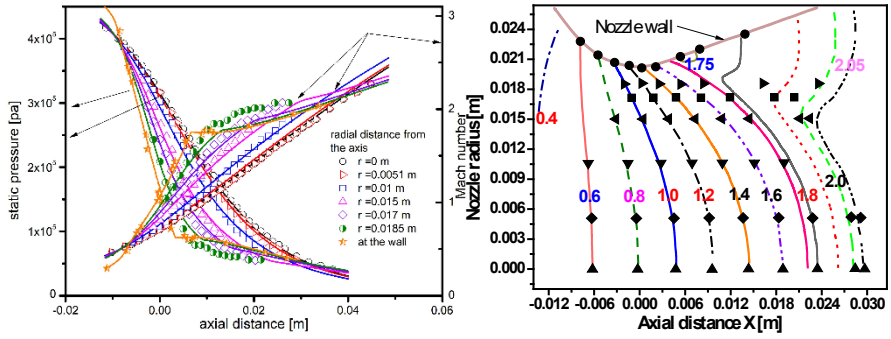

Fig. 1. Comparison of the numerical prediction with experimental data (symbols) in the transonic region: (a) Mach number and static pressure, (b) Mach contours, Exp of Cuffel et al. (1968).

Case Number	Chamber temperature (K)	Chamber pressure (bar)
Case1	$T_0 = 843$	$P_0 = 5.18$
Case2	$T_0 = 572$	$P_0 = 17.49$
Case3	$T_0 = 835$	$P_0 = 3.08$

Table 1. Different test cases

3.2 Effects of specific heat ratio on separation and static wall pressure

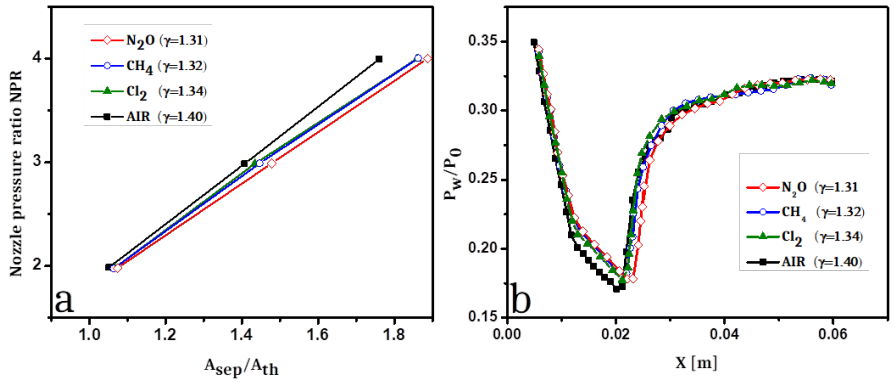

Fig. 2. Effect of γ on (a) the location of separation, (b) the distribution of wall static pressure.

This part discusses how the specific heat ratio (γ) affects the separation position of the boundary layer. The results are shown in Fig. 2, where (a) shows the separation location and (b) the static wall pressure distribution.

However, it is difficult to isolate the effect of the specific heat ratio, as other variables such as specific heat and molar mass also play an important role. To solve this problem, a cold temperature of 300 K is used to suppress the temperature dependence of specific heat, and a power law equation ($\mu/\mu_0 = (T/T_0)^m$) is applied to avoid the effects of viscosity.

In Fig. 2a, increasing the value of γ led to an observed downstream shift in the separation location. However, further information was required as both specific heat and specific heat ratio were involved. To better understand these observations, air and N_2O gas were compared as they have identical values for specific heat.

Similar conclusions were drawn when the stagnation pressure was increased as before; however, there is now no difference between the air and N_2O gases in terms of their behavior in relation to the change in γ value.

Furthermore, Fig. 2b reveals that decreasing the value of γ leads to an increase in wall pressure.

Gas	m	R	C_p	γ
N_2O	0.89	189	798.6	1.31
CH_4	0.87	518	2136.7	1.32
Cl_2	1	117	461.1	1.34
Air	0.67	287	1004.5	1.4

Table 2. Physical properties of different gases.

In Fig. 3.a, the effect of γ on the location of the detachment point was examined with gases with γ ranging from 1.3 for CH_4 to 1.66 for helium gas. The physical properties of the gases (Cp, γ, μ, λ) vary with temperature.

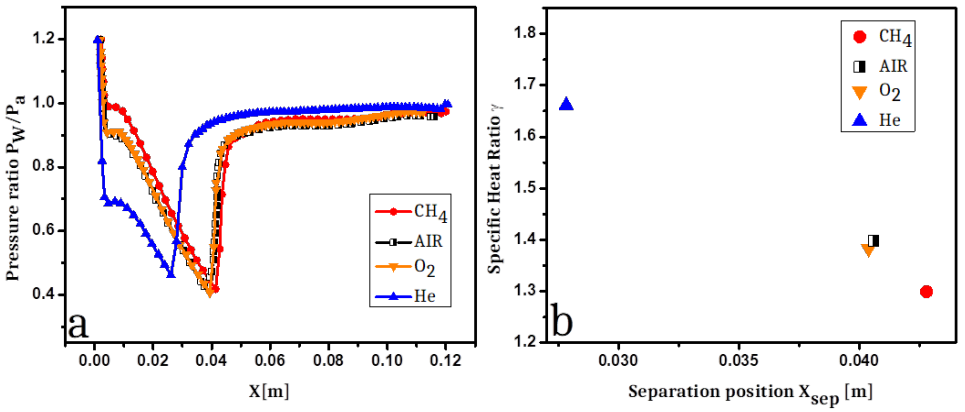

Fig. 3. (a) Wall static pressure distribution, (b) Effect of gas nature on the position of separation.

The examination of Fig. 3a, with a closer zoom, reveals that the position of boundary layer separation moves upstream for an increase in γ. In other words, this position moves downstream when γ decreases. The exact detachment point positions are shown in Fig. 3b which illustrates significant differences between helium and CH_4 as high as about 35%. These results demonstrate that real physical quantities such as Cp, γ, μ and conductivity λ have a critical impact on accurately predicting dynamic and thermal boundary layer behavior.

3.3 Wall temperature effect on wall static pressure

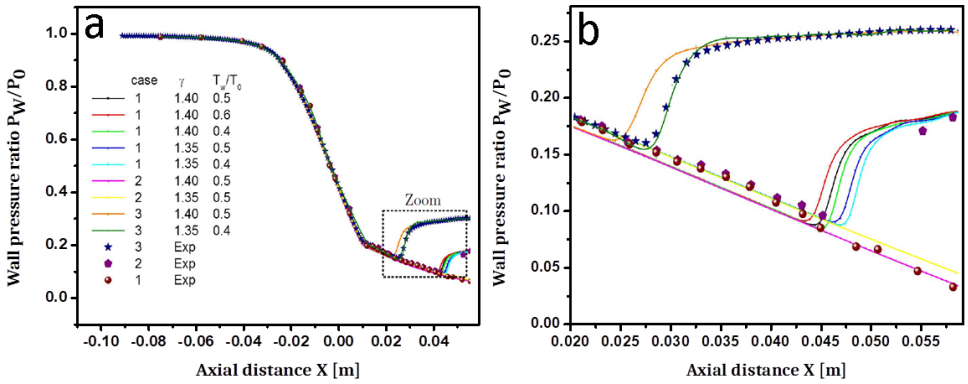

Fig. 4. (a) Wall static pressure distribution, (b) Zoom on the separation region, Exp of Back et al. (1963).

Figure 4a illustrates the normalized static wall pressure across the nozzle for different parameters, including chamber pressure and temperature (P_0, T_0), specific heat ratio γ, and wall temperature T_w. The turbulence model was validated by comparing it with the experimental data obtained by Back et al. (1963).

In Figure 4b, a closer look is taken at the separation region, where the impact of these parameters on both the wall pressure and separation points is highlighted. Additionally, this study examined how wall temperature affects performance by considering three values (T_w/T_0 = 0.4, 0.5, and 0.6) corresponding to the experiments conducted by Back et al. (1963).

This study demonstrates that increasing the wall temperature (T_W) leads to an upstream shift in the separation point. However, when T_W is too high (T_w/T_0 = 0.6), the separation point deviates from the experimental results because the temperature of the simulation is higher than the experimentally observed value of T_w/T_0 = 0.42 in the supersonic and near-separation regions. The impact of wall temperature on separation remains unclear in the literature, although some studies suggest that cold walls may result in wider separations owing to a larger wall Mach number at the initial separation points. The present findings are consistent with the experimental results reported by Délery and Marvin (1986) but differ from those found by Schmucker (1974). Schmucker's findings contradict theories about how cooler walls can lower separation pressure ratio.

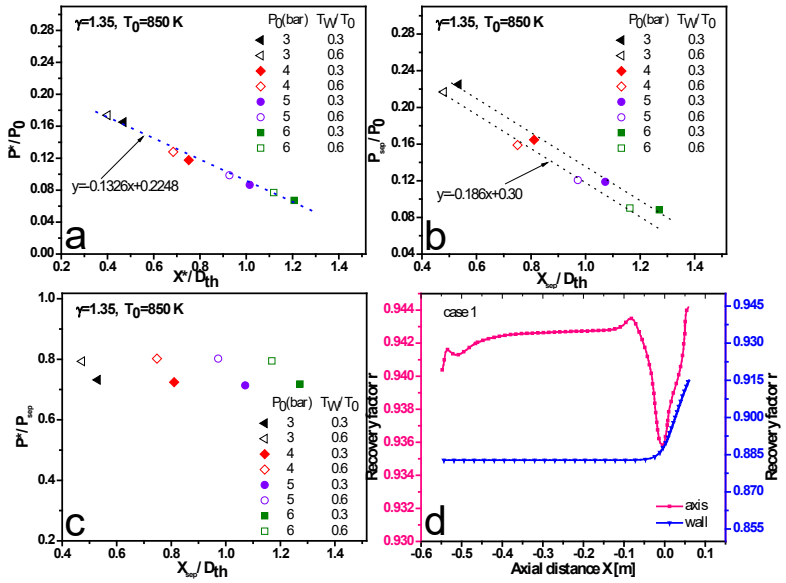

Fig. 5. Different pressure distributions: (a) pressure at the initial point of the interaction region, (b) separation pressure versus the Dimensionless separation position, (c) pressure at the initial point of the interaction region versus the dimensionless separation position, (d) the recovery factor.

Figures 5.a, 5.b and 5.c exhibit the same trend as shown in Fig. 4b. An increase in stagnation pressure leads to a downstream displacement of the separation location. When the wall temperature decreased, the separation position moved downstream at an identical chamber pressure.

The results show that $\gamma = 1.35$ yields significantly better outcomes, which is consistent with Tong and Luke (2004), and Vieser et al. (2002).

3.4 Turbulent Prandtl number effects on wall heat transfer coefficient

In this section, we investigate the wall heat-transfer coefficient h, which is defined as $h = q_w/(T_{aw} - T_w)$. To accomplish this, the walls were assumed to be adiabatic with a temperature Taw calculated using the following formula:

$$\frac{T_{aw}}{T_0} = \frac{1 + (r/2)(\gamma - 1)M^2}{1 + (0.5)(\gamma - 1)M^2}$$

The temperature recovery factor (r) is an important variable for determining the wall heat-transfer coefficient h. Figure (5d) demonstrates the variation in the recovery factor along the nozzle. According to Lebedev et al. (2006), this factor depends on several factors. Near the wall, r decreases upstream of the nozzle throat and increases just downstream, which is contrary to the heat transfer, thermal conductivity, and specific heat behaviors. However, the opposite behavior was observed along the axis because the outside boundary-layer temperature decreased. This trend can be explained by a more pronounced relaxation beyond the boundary layers. For simulation purposes, a value of r = 0.89 was used based on $r = Pr^{(1/3)}$. As shown in Fig. (6a), changing Prandtl number has a significant effect on wall heat transfer coefficient h with turbulent effects being especially noticeable in subsonic regions where increasing Pr_t leads to higher values for h.

Additional observations made in this study support the findings of Xiao et al. (2007) and Sommer et al. (1993, 1994). To gain a better understanding of the impact of the turbulent Prandtl number on the wall heat transfer coefficient, calculations were performed using variable Prt values, because a constant turbulent Prandtl number is no longer appropriate for the entire flow. The new definition for the turbulent Prandtl number used in this study is from the work of Ljuboja and Rodi (1981):

$$P_{rt} = 0.67\frac{1+0.67f}{1+0.5f}(1+0.167f)$$

With

$$\begin{cases} f = min(R_t/3.72R_k, 1) \\ R_t = k^2/\epsilon\mu, R_k = \sqrt{k}yl/\mu \end{cases}$$

Figure 8a illustrates the calculated turbulent Prandtl number, whereas Fig. 8b displays the computed wall heat transfer coefficient h for fixed and variable Prandtl numbers. The results indicate that the subsonic region is less affected because only a small decrease in the Prandtl number can be observed close to the wall boundary layer. However, major differences are seen downstream, particularly before the throat, where there is a significant drop in the Prandtl number far away from the wall. These differences start diminishing when moving downstream towards divergent section.

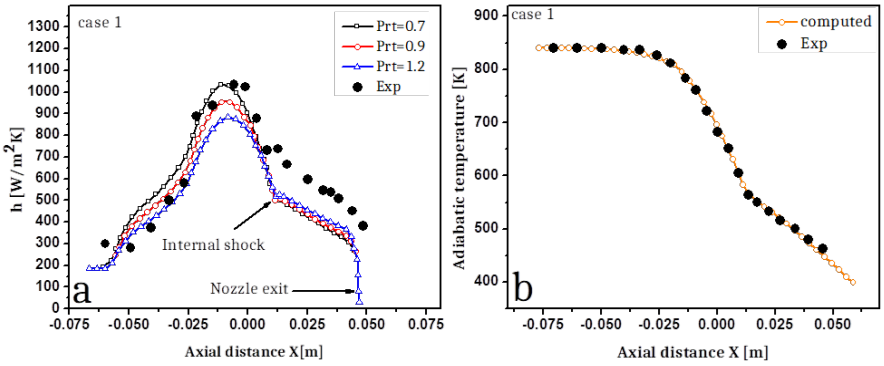

Fig. 6. (a) Heat transfer coefficient with different Prt values, (b) comparison of calculated adiabatic wall temperature against experimental data of Back et al. (1963).

Figure 6b shows good agreement between the predicted adiabatic wall temperature and the experimental results of Back et al. (1963). This agreement allows us to conclude that the differences in the heat transfer coefficient observed earlier are likely due to variations in the wall temperature distribution and calculated heat transfer through the wall.

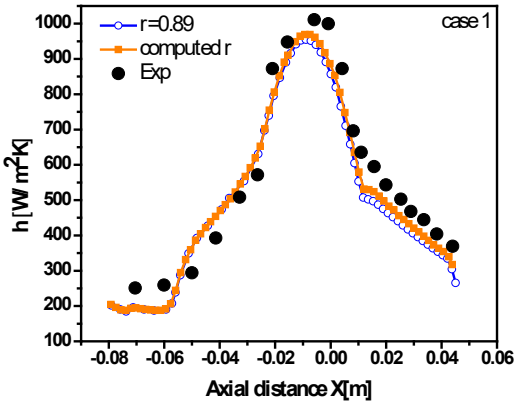

Fig. 7. Heat transfer coefficient with different *r* configurations, Exp of Back et al. (1963).

For Case 1, the wall temperature was found to vary over a range exceeding 100 Kelvin (K), especially in the critical throat region. Using the experimental wall temperature values corrects this issue by lowering the observed maximum heat transfer by approximately 30%.

Figure 7 shows the distribution of the heat transfer coefficient along the nozzle for Case 1 using the computed and fixed recovery factors. The results are in good agreement with the experimental data from Back et al. (1963), particularly in subsonic regions.

However, downstream of the internal shock wave, a significant difference was observed between the two recovery factors. It is important to note that these differences arise from several factors. First, it uses a fixed wall temperature along with the computed wall heat transfer flux, which involves various parameters including specific heat that changes along the flow field.

Moreover, the turbulence model plays an important role in accurately determining turbulent growth in supersonic regions because the boundary layer growth is significantly affected by internal shock waves, as shown in Fig. 7.

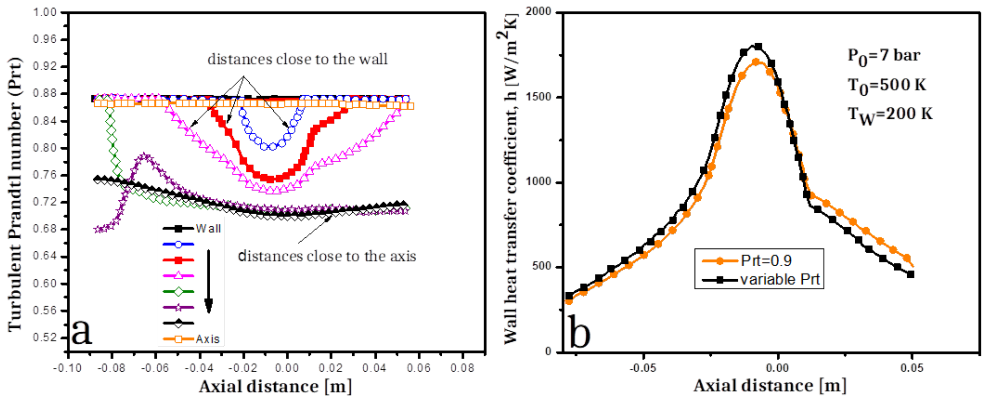

Fig. 8. (a) Distribution of variable Pr_t, (b) Effect of Pr_t variation on the distribution of wall heat flux.

3.5 Effects of wall temperature and specific heat ratio on wall heat transfer coefficient

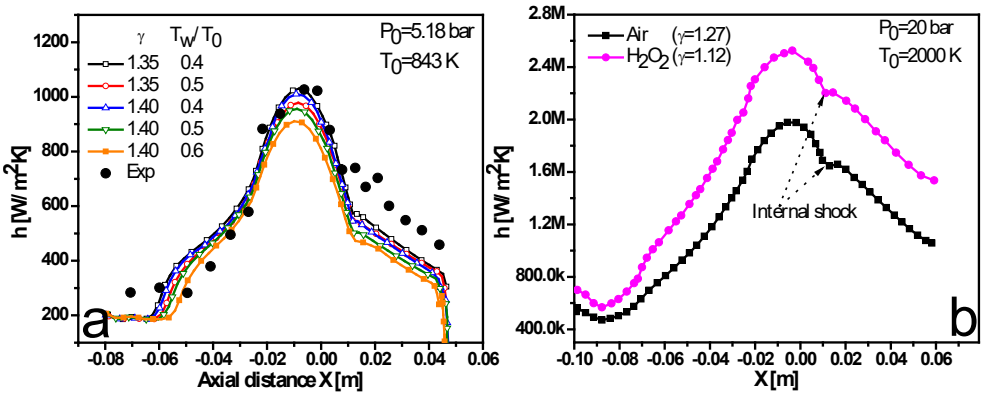

Fig. 9. Effect of (a) the wall temperature and (b) specific heat ratio (gas nature), on the distribution of wall heat transfer coefficient, Exp of Back et al. (1963).

A decrease in the wall temperature led to a slight increase in the wall heat flux, as shown in Fig. 9a. This behavior can be attributed to the dependence of the heat transfer flux on the temperature difference between the wall and core flow.

The effects of the specific heat ratio are shown in Fig. 9b, where an increase is observed in the rate of heat transfer flux due to an immediate decrease in the specific heat ratio.

3.6 Effects of chamber pressure and temperature

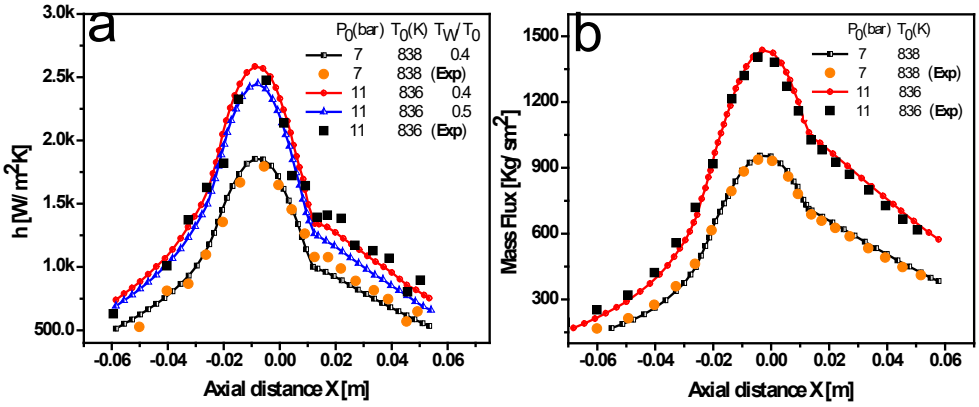

Fig. 10. (a) Effect of the stagnation pressure on the wall heat coefficient, (b) Effect of stagnation pressure on the mass flux distributionat the edge of the boundary layer, Exp of Back et al. (1963).

Numerous studies (e.g. Leccese et al. 2018, Betti et al. 2014) showed that the heat transfer coefficient increased with an increase in the chamber pressure, as shown in Fig. 10a. This was due to the resultant increase in the mass flow rate (Fig. 10b) caused by the increase in the total pressure P_0.

The maximum value of the heat transfer agrees well with that of the mass flow rate, and it is located upstream of the throat, as shown in Fig. 10b. The effect of increasing chamber temperature is less clear for low chamber pressures but worth noting that heat transfer coefficient decreases when temperature increases.

4. Conclusions

This study investigated the effects of various parameters on the thermal and dynamic properties of the flow in regenerative-cooled nozzles. The computed results reveal several important findings.

I. Using a reduced nozzle radius, the curvature ratio resulted in radial flow deviations with a higher Mach number at the wall than at the axis.

II. Increasing the Reynolds number through the inlet chamber pressure change resulted in an increase in the wall heat-transfer coefficient owing to the higher mass flow rate.

III. Modifying the chamber temperature primarily affected the mass flow rate, with an anticipated increase in heat transfer coefficients for higher stagnation pressures, but a less evident relationship for lower stagnation pressures.

IV. Changes in the specific heat ratio (γ) affected the separation location and static pressure on the wall.

V. The heat transfer distribution following an unfavorable gradient pressure was influenced by the boundary layer pattern and the designated wall temperature.

VI. The maximum area of the heat transfer coefficient was located upstream of the throat at the position of maximum mass flow rate.

VII. This study showed that wall temperature had significant impact on heat-transfer rate, wall pressure and location of detachment flow. The results were consistent with existing experimental data, indicating good agreement between qualitative simulations and experimental observations across different configurations.

Overall, this research provides valuable information about heat transfer rates and separation flows for various configurations and sheds light on poorly understood parameters, such as the impact of stagnation temperature on the heat transfer rate or the effect of wall temperature on the separation position.

Nomenclature

C_p	Specific heat at constant pressure [J/KgK]	S_{ij}	strain tensor [1/s]
C_v	Specific heat at constant pressure [J/KgK]	M	Mach number
T	Temperature [K]	u_i, u_j, u_k	Mean velocities [m/s]
R	Gas constant [J/KgK]	p_{r_t}	Turbulent Prandtl number
Ω	Scalar measure of vorticity tensor [1/s]	h	Heat transfer coefficient [W/m^{2}K]
Ω_{ij}	vorticity tensor [1/s]	E	Total energy [J/Kg]
μ_t	Turbulent eddy viscosity [Kg/ms]	F_1, F_2	Auxiliary functions

μ	Dynamic viscosiy [Kg/ms]	A_Ω, A_S, A_0	Realizability constants
k	Turbulence kinetic energy [m^2/s^2]	F	Convective flux vector [Kg/sm2]
ω	Specific dissipation rate [1/s]	F_v	Viscous flux vector [Kg/sm2]
x_i, x_j	Spatial coordinates [m]	a_1	Bradshow constant
ρ	Density [Kg/m^3]	Subscripts	
γ	Specific heat ratio	0	Nozzle entrance codition
r	Radius [m], radial coordinate [m], recovery factor	$*$	Initial point at the interaction region
P, p^*	Pressure and effective pressure [N/m^2]	Sep	Separation position
t	Time [s]	w	Wall position
S	Scalar measure of strain tensor [1/s]	aw	Adiabatic wall
NPR	Chamber to ambient pressure	th	Throat position

References

Arnold R., Suslov D. and Author C. (2009). Inuence Parameters on Film Cooling Effectiveness in a High Pressure Subscale Combustion Chamber, 47th AIAA Aerospace Sciences Meeting including The New Horizons Forum and Aerospace Exposition. Orlando, Florida. https://doi.org/10.2514/6.2009-453.

Back L.H., Massier P.F. and Gier H.L. (1964). Convective Heat Transfer in a Convergent-Divergent Nozzle, *Int. J. Heat Mass Transfer*, 7, 549–568. https://doi.org/10.1016/0017-9310(64)90052-3.

Baron J.R. and Durgin F.H. (1954). An experimental investigation of heat transfer at the boundaries of supersonic nozzles, WADC TR 54-541, NavalSupersonic Laboratory, Massachusetts institute of technology, WADC Technical Report 54-541.

Bensayah K., Kamri K. (2022). Numerical investigation of supersonic flow separation in thrust-optimized contour rocket nozzle, *Journal of the Serbian Society for Computational Mechanics*, 16(2), 43-55. 10.24874/jsscm.2022.16.02.03.

Bensayah K., Hadjadj A. and Bounif A. (2014). Heat Transfer in Turbu- lent Boundary Layers of Conical and Bell Shaped Rocket Nozzles with Complex Wall Temperature, *Numerical Heat Transfer part-A,* 66(3),289–314. http://dx.doi.org/10.1080/10407782.2013.873283.

Betti B., Bianchi D., Nasuti F. and Martelli E. (2014). Chemical Reaction Effects on Wall Heat Flux in Liquid Rocket Thrust Chambers, 50th AIAA/ASME/SAE/ASEE Joint Propulsion Conference Cleveland, OH. https://doi.org/10.2514/6.2014-3675.

Campbell C. and Farley J. (1960). Performance of several conical convergent-divergent rocket type exhaust nozzles, NASA, TN D-467.

Cuffel R.F., Back L.H. and Massier P.F. (1968). Transonic Flow-field in a Supersonic Nozzle with Small Throat Radius of Curvature, *AIAA Journal*, 7(7), 1364–1368. https://doi.org/10.2514/3.5349.

Daimon Y., Negishi H., Yamanishi N., Nunome Y., Sasaki M. and Tomita T. (2012). Combustion and Heat Transfer Modeling in Regeneratively Cooled Thrust Chambers (Optimal Solution Procedures for Heat Flux Estimation of a Full- Scale Thrust Chamber), 48th AIAA/ASME/SAE/ASEE Joint Propulsion Conference and Exhibit, Joint Propulsion Conferences, DOI:10.2514/6.2012-4009.

Délery J. and Marvin J. (1986). Shock-Wave boundary layer Interactions, volume AGAR-Dograph N. 28, AGARD.

Frank G. and Pfitzner M. (2017). Investigation of the heat transfer coefficient in a tran- spiration film cooling with chemical reactions, *International Journal of Heat and Mass Transfer*, 113, 755-763. https://doi.org/10.1016/j.ijheatmasstransfer.2017.05.103.

Kim J.G., Lee J.W. and Kim K.H. (2012). Investigation on the Characteristics of Plume-Induced Flow Separation and Wall Heat Transfer, *Journal of Spacecraft and Rockets*, 49(1), 189–192. https://doi.org/10.2514/1.51782.

Kolozsi J.J. (1958). An Investigation of Heat Transfer through the Turbulent Boundary Layer in an Axially Symmetric Convergent-Divergent Nozzle, MS Thesis, Ohio State University, Columbus, OH, 1958.

Kurtbas I. (2008). The effect of different inlet conditions of air in a rectangular channel on convection heat transfer: Turbulence flow, *Experimental Thermal and Fluid Science*, 33(I1), 140-152 https://doi.org/10.1016/j.expthermflusci.2008.07.012.

Leccese G., Bianchi D., Betti B., Lentini D. and Nasuti F. (2018). Convective and Radiative Wall Heat Transfer in Liquid Rocket Thrust Chambers, *Journal of Propulsion and Power*, 34(2), 318–326. https://doi.org/10.2514/1.B36589.

Lebedev V.P., Lemanov V.V. and Terekhov V.I. (2006). Film-Cooling Efficiency in a Laval Nozzle Under Conditions of High Freestream Turbulence, *Journal of Heat Transfer*, 128(6), 571-579. https://doi.org/10.1115/1.2188508.

Ljuboja M. and Rodi W. (1981). Prediction of Horizontal and Vertical Turbulent Buoyant Wall Jets, *J. Heat Transfer*, 103(2), 343–349. https://doi.org/10.1115/1.3244464.

MacCormack R.W. (1985). Current status of numerical solution of the Navier-Stokes equations, *AIAA journal*, https://doi.org/10.2514/6.1985-32.

Miranda A. and Naraghi M. (2011). Analysis of Film Cooling and Heat Trans- fer in Rocket Thrust Chamber and Nozzle, 49th AIAA Aerospace Sciences Meeting including the New Horizons Forum and Aerospace Exposition. Orlando, Florida. https://doi.org/10.2514/6.2011-712.

Ragsdale W.C. and Smith J.M. (1959). Heat transfer in nozzles, *Chemical Engineering Science*, 11(4), 242–251. https://doi.org/10.1016/S0009-2509(15)30003-8.

Saunders O.A. and Calder P.H. (1953). Heat Transfer in a Nozzle at Supersonic Speeds, Proceedings of the Institution of Mechanical Engineers, Part B: Management and engineering manufacture, 167(1b), 232–239. https://doi.org/10.1177/002034835316701b16.

Schmucker R.H. (1974). Status of flow separation prediction in liquid propellant rocket nozzles, Technical Memorandum TM X-64890. NASA, George C. Marshall Space Flight Center.

Sommer T.P., So R.M.C. and Zhang H.S. (1993). A Near Wall Variable Turbulent-Prandtl-Number Turbulence Model For Compressible Flows, *AIAA*, 31(1), 27-35. https://doi.org/10.2514/3.11314.

Sommer T.P., So R.M.C. and Zhang H.S. (1994). A Near Wall Four-Equation Turbulence model for Compressible Boundary Layers, NASA Contractor Report (NASA-CR-4436), Arizona State Univ.

Steger J. and Warming R.F. (1979). Flux vector splitting of the invisid gas dynamics equations with application to finite difference methods, NASA, TM-78605. https://doi.org/10.1016/0021-9991(81)90210-2.

Tong X.L. and Luke E. (2004). Turbulence Models and Heat Transfer in Nozzle Flows, *AIAA*, 42(11),2391-2393. https://doi.org/10.2514/1.8900.

Vieser W., Esch T. and Menter F. (2002). Heat Transfer Predictions Using Advanced Two-Equation Turbulence Models, CFX/ANSYS, Tech. Rept. CFX-VAL 10/0602, Otterfing, Germany.

Xiao X., Hassan H.A. and Edwards J.R. (2007). Role of Turbulent Prandtl Numbers on Heat flux at Hypersonic Mach Numbers, *AIAA*, 45(4), 806–813. https://doi.org/10.2514/1.21447.